separations

MDPI

Article

Enhanced CO_2 Capture by Sorption on Electrospun Poly (Methyl Methacrylate)

Michele Ciulla, Valentino Canale, Rafal D. Wolicki, Serena Pilato, Pantaleone Bruni, Stefania Ferrari, Gabriella Siani, Antonella Fontana and Pietro Di Profio *

Department of Pharmacy, University of Chieti-Pescara "G. d'Annunzio", via dei Vestini, I-66100 Chieti, Italy; michele.ciulla@unich.it (M.C.)

* Correspondence: pietro.diprofio@unich.it

Abstract: Poly(methyl methacrylate) (PMMA) is characterized by high CO_2 capture yield under mild pressures and temperatures. A morphological modification of powdery amorphous PMMA (pPMMA) is carried out by electrospinning to increase the surface/volume ratio of the resulting electrospun PMMAs (ePMMAs). This modification improves the kinetics and the capture yields. The rate constants observed for ePMMAs are two to three times higher than those for pPMMA, reaching 90% saturation values within 5–7 s. The amount of sorbed CO_2 is up to eleven times higher for ePMMAs at 1 °C, and the highest difference in captured CO_2 amount is observed at the lowest tested pressure of 1 MPa. The operating life of the ePMMAs shows a 5% yield loss after ten consecutive runs, indicating good durability. Spent electrospun PMMAs after several cycles of CO_2 sorption-desorption can be regenerated by melting and again electrospinning the molten mass, resulting in a CO_2 capture performance that is undistinguishable from that observed with fresh ePMMA. Scanning electron and atomic force microscopies show a reduction in surface roughness after gas exposure, possibly due to the plasticization effect of CO_2. This study shows the potential of electrospun PMMAs as solid sorbents for carbon capture from natural gas or pre-combustion and oxyfuel combustion processes.

Keywords: CO_2 capture; solid sorbents; poly (methyl methacrylate); polymer plasticization; electrospinning; natural gas

Citation: Ciulla, M.; Canale, V.; Wolicki, R.D.; Pilato, S.; Bruni, P.; Ferrari, S.; Siani, G.; Fontana, A.; Di Profio, P. Enhanced CO_2 Capture by Sorption on Electrospun Poly (Methyl Methacrylate). *Separations* **2023**, *10*, 505. https://doi.org/10.3390/separations10090505

Academic Editor: Moises Bastos-Neto

Received: 3 August 2023
Revised: 1 September 2023
Accepted: 8 September 2023
Published: 14 September 2023

1. Introduction

Climate change has become one of the most alarming issues that our society ever faced, urging the development of green alternatives to fossil fuels. However, the transition to fully renewable energy sources is slow, and the combustion of oil and gas is still the main source of our energy needs. In this scenario, it is crucial to develop efficient and sustainable technologies for Carbon Capture and Storage (CCS), which relates to the body of technologies devised to capture anthropogenic carbon dioxide. These techniques can be roughly divided into (i) post-combustion capture, where the gas is captured at the end of a combustion process; (ii) pre-combustion capture, where the fossil fuel is partially oxidized in order to form a syngas mix, and CO_2 is then separated therefrom; (iii) oxy-fuel combustion, where the fossil fuel is burned into an oxygen-enriched atmosphere, thus increasing the amount of CO_2 produced and making the process of extraction easier [1,2].

At present, the most advanced technologies relating to CO_2 mitigation are focused on post-combustion processes, where the flue gas is processed for CO_2 removal under low pressures. Traditional methods for CO_2 capture under ambient pressures are based on amine-based solvents. In comparison to other capture methods, the employment of chemical absorption through amines in post-combustion settings can directly extract carbon dioxide from flue gas, and is readily adapted to common power plants [3]. However, other CO_2-containing gas mixtures (e.g., pre-combustion and oxyfuel combustion, as well as natural gas) are processed under higher pressures, where polymeric membranes

seem cheaper and more effective than liquid sorbents [4]. A recent review reports on the major challenges in the application of polymer membranes for CO_2 separation [5]. One interesting material in this regard is poly(methyl methacrylate) (PMMA), whose swelling and sorption properties have been comprehensively studied by Wissinger in 1987 [6,7]. Those studies show a remarkable sorption behavior under a range of CO_2 pressures (0.1–10 MPa) and good swelling abilities [6,8–10], displaying higher affinity between PMMA and carbon dioxide as compared to other polymers [11,12] Due to this ability, which is also typical of other materials [13], PMMA has been also studied in foaming processes [14–16]. The solubility of high-pressure carbon dioxide into PMMA depends on the operating temperature and pressure. Specifically, subcritical carbon dioxide increases its solubility in the polymer as the temperature decreases [6,8,17–20]. The interaction between the polymer side chains, composed of a methyl ester, and CO_2 was studied, *inter alia*, by ab initio calculations, FT-IR spectroscopy, and Raman spectroscopy, showing that the carbonyl group is involved in a Lewis acid-base relation with CO_2 [18,21–25]. The interaction is extremely dynamic and is dependent on pressure and temperature [26]. Also, considering the Flory-Huggins parameter in the study of the interactions between the polymer and a penetrant gas, it was shown that their interaction is stronger at lower temperatures [27]. The interaction and penetration of the gas into PMMA are characterized by both a Fickian diffusion of the gas within the rubbery region of the polymer and a non-Fickian behavior when PMMA is in the glassy state, possibly also affected by the relaxation that occurs during its plasticization by CO_2 [28].

Most polymers show a glass transition phenomenon, which is characterized by a couple of temperature and pressure values at which the polymer shifts from glassy to rubbery form [29–31]. One of the most interesting aspects of the CO_2 sorption properties of PMMA is its so-called *retrograde vitrification*, according to which—under certain pressures—the polymer exists in a rubbery state at low and high temperatures, and in a glassy form at intermediate temperatures [32]. The transition between the glassy and rubbery forms of the polymer depends mostly on the temperature, but there is also a contribution from the gas pressure and the inherent plasticizing property of carbon dioxide. In a plot of the state of the polymer as a function of temperature and pressure, the phenomenon of retrograde vitrification causes the split of the curve basically in three regions defined by the transitions from rubbery to glassy states [32–38]. These phase changes were also characterized by Raman spectroscopy [23], and this technique basically agrees with gravimetric and calorimetric measurements in the determination of the plasticization phenomenon induced by CO_2. Also, time-resolved Raman shifts can be used to derive the gas sorption kinetics [39,40]. Considering that the glassy and rubbery forms of PMMA have different CO_2 sorption characteristics, it is important to recognize these forms during the CO_2 capture process in order to explain the sorption profiles of PMMA. Particularly important is the alteration of other properties of the polymer, such as the heat capacity, heat of sorption, and plasticization caused by CO_2 [41–43]. It is known that the plasticization of the polymer by carbon dioxide is more pronounced at lower temperatures (due to an increase in CO_2 solubility) [44], and this increased plasticization is paralleled by the transition into the rubbery state and a general decrease in T_g [34].

Due to the interaction properties of PMMA with CO_2, as summarized above, PMMA may be developed into a carbon capture medium in practical applications requiring CO_2 removal from gas mixtures, such as oxy-fuel, biogas, syngas, and natural gas. PMMA was also used in co-polymer membranes, and PMMA hybrid membranes containing AgCl nanoparticles [45,46]. While the use of membranes is effective, they show some limitations from an industrial standpoint, such as high working pressures and low resistance to mechanical stress.

In the present work, we have addressed some of the above issues, with the aim to improve the CCS performance and life cycle of PMMA through structural modification by electrospinning, which enabled us to fabricate oriented polymer fibers from commercial

PMMA powder. Electrospun fibers were also examined by AFM, FT-IR, SEM, TGA, and BET analyses.

2. Experimental Section

2.1. Chemicals and Materials

Amorphous poly (methyl methacrylate) (pPMMA), average M_w 120.000, and anhydrous N,N-Dimethylformamide (DMF, 99.8%) were purchased from Sigma-Aldrich (Mailand, Italy). SS-grade CO_2 (>99.8% CO_2) was obtained from SOL S.p.A. (Monza, Italy).

Electrospun PMMAs (ePMMAs) were made as follows: the polymer powder was solubilized (31 wt%) into DMF by magnetic stirring at 28 °C for 18h at 250 RPM. The electrospinning apparatus that was used is schematically described in [47]. The solution was electrospun by placing the metal needle in a vertical arrangement with respect to the steel collector, which was suitably covered with aluminium foil and kept at a distance of 21–22 cm. Temperature, relative humidity, and solution flow were fixed at 28 °C, 35% RH, and 1.5 mL/h, respectively, throughout the process. The polarity of the electric field was set and directed from positive to negative charge for ePMMA+, and from negative to positive for ePMMA-. The DC voltage applied to the first and second sample types were 12 kV and 15 kV, respectively. Recycled electrospun membranes were also made by recovering exhausted PMMAs used for gas sorption experiments, and using the same procedure and parameters described above.

2.2. Experimental Apparatus

The experimental apparatus for gas sorption measurements is shown in Figure 1 and is based on a previously described device with slight modifications [48–50]. The reaction chamber was a small AISI 316L stainless-steel reactor, with an internal volume of 10 mL and an operating pressure of up to 6 MPa. The temperature was controlled using a chiller unit with a cooling power of 1000 W, which was also used for controlling the temperature of the gas line from the mass flow meter to the reactor. The gas flow was measured using an F131 M series thermal mass flow meter (Bronkhorst High-Tech B.V. Ruurlo, The Netherlands) with a measuring range of 1–100 NmL/min and an operating pressure of up to 20 MPa. Gas inflow readings can be directly converted into gas moles through the integration of flow/time curves. This approach allowed the measurement of both the kinetics of the process and the equilibrium amounts of sorbed carbon dioxide. Proper control of the input gas pressures was achieved through a Tescom CC Series micrometering valve (Emerson, St. Louis, MO, USA). Gas pressures within the reactor were measured with a 4–20 mA pressure transducer (Gems Sensors & Controls; Brighton, UK) with a measuring range of 0–10 MPa. The reactor was equipped with two resistive temperature detectors (RTD) PT100 class 1/3 DIN purchased from OMEGA Engineering, Inc. (Norwalk, CA, USA). A custom-built process controller was assembled to record the pressure, temperature, and gas flow by using an ELCO Top 7 PLC (ELCO, Schio, Italy).

2.3. Determination of CO_2 Capture

Into the reactor, 1.00 g of powder or electrospun PMMA was introduced. The system was set at a temperature setpoint for about 5 min before charging with the gas. The reactor chamber was connected to a line vacuum system (0.02 MPa) to remove atmospheric air. During this evacuation, the CO_2 introduction valve was opened for short periods to introduce small amounts of carbon dioxide into the chamber. Then, the gas was introduced into the reactor up to the target pressure. The CO_2 flux at the beginning was at 400 NmL/min and then decreased following a PID algorithm. After the pressure setpoint was reached (1, 2, 3, and 4 MPa at 20 °C; 1, 2, and 3 MPa at 1 °C; 4 MPa was not tested at 1 °C because of CO_2 liquefaction), the CO_2 influx data from the flowmeter were recorded. The two temperatures adopted in this work (20 °C and 1 °C) were chosen with the aim of gathering information on the temperature dependency of CO_2 solubility in the polymer while remaining within

the glassy region of PMMA. Also, these T/P values are compatible with the ranges for some industrially relevant processes, such as the removal of CO_2 from natural gas [51].

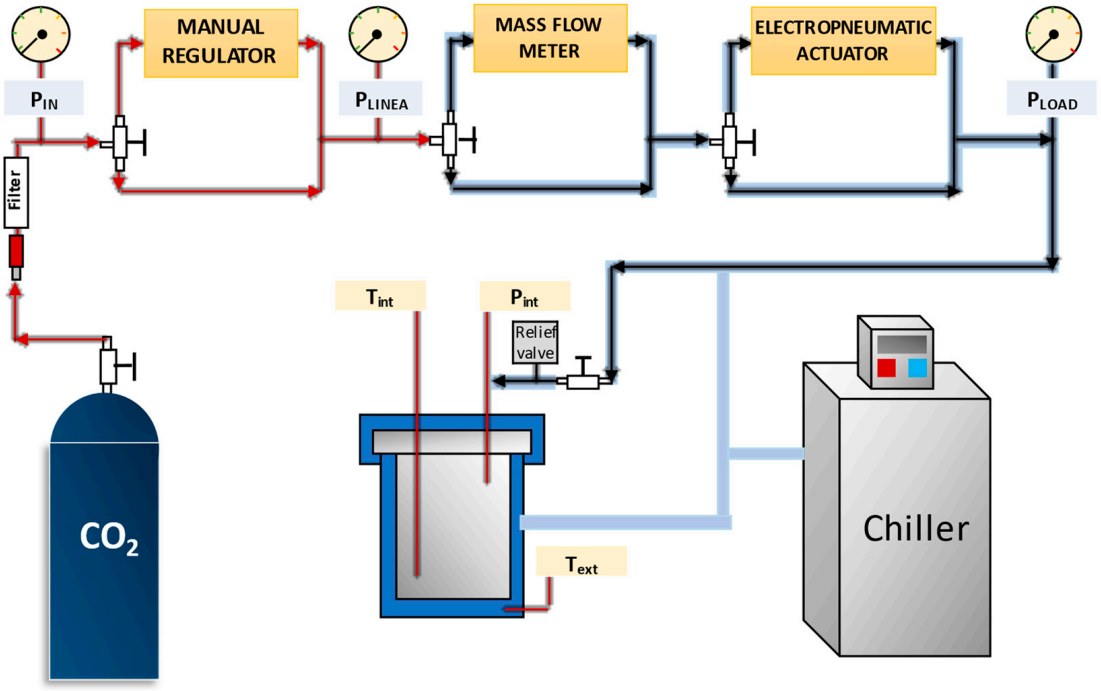

Figure 1. Schematics of the experimental apparatus.

With the aim to consider only the gas that interacts with the polymer, a preliminary reference experiment was run to measure the volume of gas inside the reactor while it was filled with inert material having the same volume as the PMMA sample. Then, using arithmetical manipulation, we obtained the exact gas amount. Sample densities were measured using a helium pycnometer. After a sorption cycle, the pPMMA sample was degassed for 30 min at 1.7 kPa (line vacuum) before subjecting it to the next sorption step.

All sorption profiles were consistent with the apparent first-order kinetics, according to the rate law:

$$\text{rate} = d[CO_2]/dt = k_{obs}[CO_2].$$

k_{obs} values were obtained using a least-squares fitting of the experimental data.

2.4. Method Validation

The validation was performed under selected pressures (1, 2, 3, and 4 MPa), temperatures (1 °C, 20 °C), and volumes, by comparing gas flow readings to gravimetric measurements, carried out by weighing sorbed CO_2 amounts with an analytical balance. The method could be considered validated since the weight measured in this way differed by $\leq$0.5 wt% from the mass calculated from the flowmeter. The accuracy of the flowmeter measurements was $\pm$0.5% of reading (Rd), whereas repeatability was <0.2% Rd.

2.5. Brunauer–Emmett–Teller (BET) Analysis

The isotherms were acquired using the ASAP 2020 Plus adsorption analyzer from Micromeritics, equipped with high-accuracy pressure transducers (precision 0.15% of absolute pressure reading) allowing for measurements in nitrogen at 77 K. Before sorption analysis, the sample was degassed at a temperature of 70 °C for 12 h under ultrahigh vacuum. Relative pressure points P/P_0 in the range 0.0001–0.01 were included to assess the extent of any microporosity within the samples. BET surface area was calculated over a nominal pressure range of 0.05–0.25.

2.6. Scanning Electron Microscopy

SEM micrographs were acquired by using the Phenom XL Desktop apparatus. Images were obtained under high vacuum (1Pa) in backscatter mode with an optical magnification of 10,000× and acceleration voltages of 15KV. The images were analyzed using the Phenom ProSuite software to obtain information on fiber sizes. Each sample was sputtered with a very thin layer of gold in order to improve the resolution using an Electron Microscopy Sciences SEM K550 sample preparation sputter coater.

2.7. AFM Analysis

AFM in tapping mode was used for the morphological characterization at a nanoscale level of the PMMA fibers, before and after the cycles of CO_2 sorption. The analyses were conducted on pristine and exhausted ePMMA+ and ePMMA- samples using a Multimode 8 AFM (Bruker Corp., Billerica, MA, USA) with a Nanoscope V controller and a J scanner. Tapping mode measurements were performed using a rectangular cantilever RTESPA-150, which had a resonance frequency and spring constant of 150 kHz and 5 N/m, respectively. The mats of the PMMA fibers were fixed on an adhesive substrate, and multiple scans of single fibers were taken for each sample. Roughness calculations were performed using the software Nanoscope Analysis 1.8 (Bruker Corp., Billerica, MA, USA), and the average roughness (Ra) and root mean square roughness (Rq) parameters were used to describe the surfaces of the fibers.

2.8. TGA Analysis

Thermogravimetric analyses were conducted on a PerkinElmer STA6000 (PerkinElmer SpA, Milan, Italy) using Pyris software. The TGA curves of the electrospun negative (grey line), positive (red line), and powder (blue line) PMMAs are shown in part c of Section 3.2. Each sample was heated under a nitrogen flow of 20 mL/min at a rate of 10 °C/min to 700 °C with a final isotherm of 15 min.

2.9. FT-IR Analysis

IR spectra were taken using a Shimadzu IRAffinity-1S FTIR spectrophotometer (Shimadzu Italia S.r.l., Milan, Italy) equipped with a sealed and desiccated interferometer, a DLATGS (Deuterated Triglycine Sulphate Doped with L-Alanine) detector, and a single reflection diamond ATR crystal (QATR 10, Shimadzu Italia S.r.l., Milan, Italy). Spectra were recorded in the range from 3250 to 450 cm^{-1}, co-adding 45 interferograms at a resolution of 4 cm^{-1} with Happ–Genzel apodization. The ATR crystal was carefully cleaned before each analysis, a background was recorded for each sample, and the measurements were performed in triplicate. Further description of the spectral processing is reported in the Supplementary Material.

3. Results

3.1. Sorption Experiments

a. Powder PMMA

Commercial PMMA in powder form (pPMMA) was subjected to three consecutive pressurization (sorption)/depressurization (desorption) cycles (shown as I, II, and III in the Figures) under different CO_2 pressures (1, 2, 3, and 4 MPa) and temperatures (1 °C and 20 °C). Figure 2 shows the sorption profiles of pPMMA at 20 °C and 1 °C.

At 20 °C, pPMMA shows a moderate amount of CO_2 sorption, which is proportional to the gas pressure. Under 1 MPa, only ca. 6–8 mg of CO_2 is captured by 1 g of the polymer, and this amount increases up to ca. 120–150 mg at 4 MPa (Table 1). In general, the sorption kinetics are slower for the first cycle, but the plateau values are higher than those reached from the second and successive cycles, with the latter having a faster sorption rate than the first cycle. This phenomenon is mainly due to the first-pass plasticization effect: the gas is adsorbed into the free volume between polymer chains, so that chain mobility is accelerated, dilation and deformation are enhanced, and viscosity decreases [43]. The

modifications related to plasticization increase the sorption rate of the gas after the first cycle. In particular, for the experiments at 4 MPa, a remarkable decrease in the sorption amount is observed after the first cycle when the pPMMA is degassed for 30 min at 1.7 kPa (line vacuum) before subjecting it to the next sorption step.

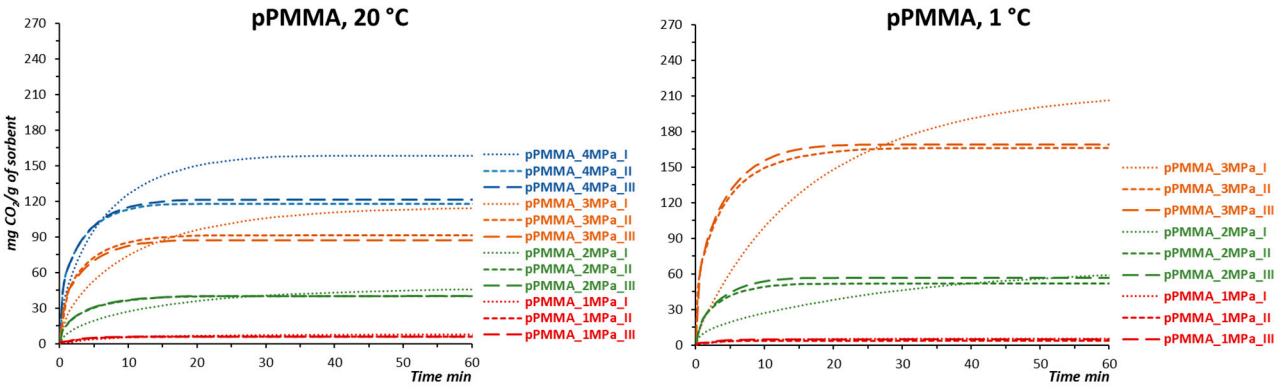

Figure 2. Kinetic profiles of CO_2 sorption by pPMMA at 20 °C and 1 °C and the indicated pressures.

Table 1. Amounts of sorbed CO_2 (in mg) for g of PMMA under the tested pressures and temperatures for three repeated cycles (I, II, and III). For each cycle (i.e., cycles I, II, and III), all the experiments were performed in triplicate.

	pPMMA					
	20 °C			1 °C		
	I	II	III	I	II	III
1 MPa	8.0 ± 1.8	6.1 ± 1.2	5.9 ± 1.3	5.3 ± 0.9	3.8 ± 0.9	4.7 ± 1.1
2 MPa	45.8 ± 1.9	40.1 ± 3.0	40.4 ± 2.4	59.3 ± 0.8	51.8 ± 1.2	56.6 ± 2.0
3 MPa	114.3 ± 3.2	91.2 ± 2.9	87.1 ± 2.7	206.3 ± 3.8	166.2 ± 3.2	168.6 ± 3.3
4 MPa	158.2 ± 2.5	118.0 ± 3.1	121.0 ± 3.1	---	---	---
	ePMMA+					
	20 °C			1 °C		
	I	II	III	I	II	III
1 MPa	46.1 ± 1.5	43.8 ± 1.3	43.6 ± 1.8	60.6 ± 1.7	64.4 ± 1.4	64.7 ± 2.0
2 MPa	84.2 ± 2.1	83.0 ± 2.2	81.7 ± 2.8	143.3 ± 3.5	134.5 ± 3.7	138.1 ± 3.3
3 MPa	124.9 ± 3.8	121.9 ± 3.5	118.4 ± 2.2	259.2 ± 4.0	223.9 ± 4.2	227.2 ± 4.6
4 MPa	142.2 ± 4.1	148.9 ± 3.6	143.9 ± 3.1	---	---	---
	ePMMA-					
	20 °C			1 °C		
	I	II	III	I	II	III
1 MPa	46.0 ± 1.0	45.9 ± 2.1	45.3 ± 1.6	56.8 ± 2.1	55.4 ± 1.4	57.0 ± 1.1
2 MPa	96.1. ± 2	91.5 ± 2.2	85.8 ± 1.9	141.4 ± 3.0	139.5 ± 2.3	134.0 ± 2.8
3 MPa	126.0 ± 2.5	114.7 ± 3.8	114.4 ± 2.1	201.7 ± 4.2	195.0 ± 4.5	201.9 ± 4.0
4 MPa	179.3 ± 3.1	156.1 ± 2.0	161.8 ± 3.6	---	---	---

The behavior of pPMMA is qualitatively similar at 1 °C, but a slight moderate increase in CO_2 sorption is observed compared to that at 20 °C. Particularly striking is the amount of CO_2 sorbed at 3 MPa/1 °C, which is approximately twice the amount at 20 °C (Table 1). This higher amount of bound CO_2 may reflect a stronger interaction at a lower T, following the Flory–Huggins interaction theory, which is known to decrease as the temperature increases [27]. Also, at 1 °C, the kinetics of the first sorption are remarkably slower than those of the subsequent cycles, but the plateau values are higher at 3 MPa. Experiments at 4 MPa/1 °C could not be performed due to the liquefaction of CO_2 (see the Experimental Section).

b. Positive electrospun PMMA (ePMMA+)

The situation is different when using ePMMA+ polymers (Figure 3), where sorption cycles are more consistent and sorbed CO_2 amounts are negligibly different among the cycles. Sorbed gas amounts increase with pressure and were higher than those measured using pPMMA. It is worth noting that the difference in the amount of sorbed CO_2 drastically increased at the lowest tested pressure (1 MPa) at both 1 °C (ca. 11-fold increase) and 20 °C (ca. 6-fold increase; see Table 1) compared to the corresponding values of pPMMA. The best performance was observed with ePMMA+ at 3 MPa/1 °C, where ca. 260 mg of CO_2 was captured using 1g of ePMMA+, qualitatively following the same overall kinetics as cycles #2 and #3.

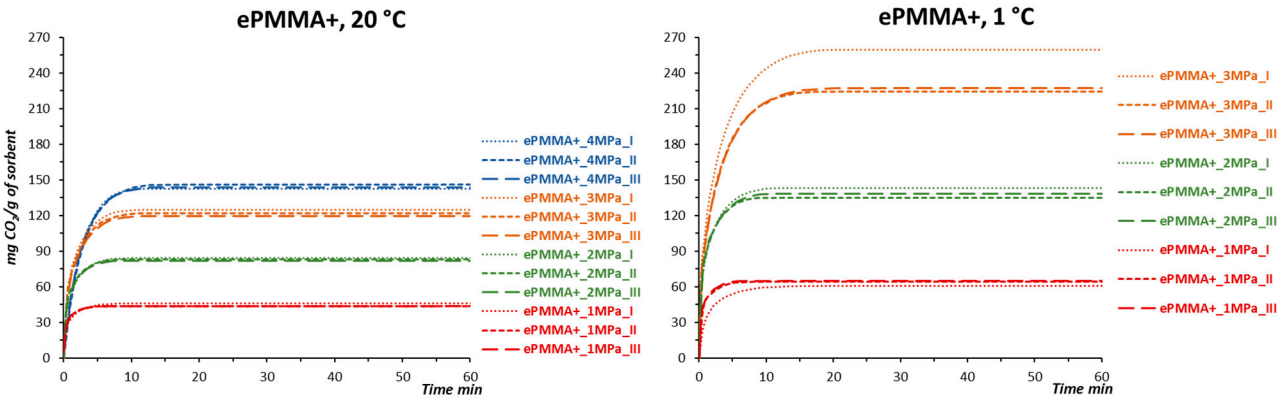

Figure 3. Kinetic profiles of CO_2 sorption by ePMMA+ at 20 °C and 1 °C, under the indicated pressures.

c. Negative electrospun PMMA (ePMMA-)

Similar findings were obtained for ePMMA- (Figure 4), where the plateau values of sorbed CO_2 are roughly close to those for ePMMA+ at 20 °C and marginally lower at 1 °C.

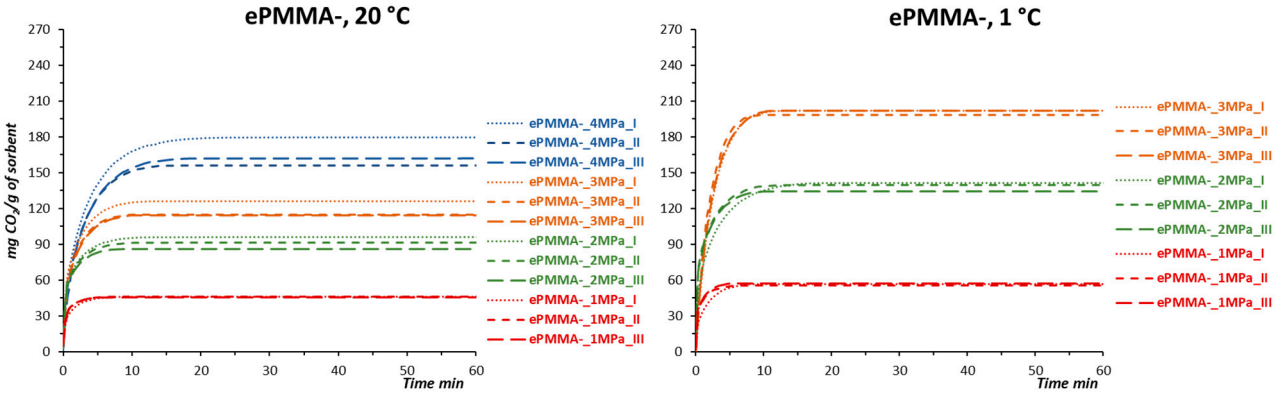

Figure 4. Kinetic profiles of CO_2 sorption by ePMMA- at 20 °C and 1 °C, under the indicated pressures.

Figure 5 shows a comprehensive comparison of the first-order rate constants (k_{obs}) for CO_2 sorption by pPMMA and ePMMAs under the tested conditions. The values of k_{obs} for ePMMAs are generally 2–3 times higher than those for pPMMA, with the fastest being observed at 1 MPa CO_2 pressure. Cycle I is much slower than cycles II and III for pPMMA under all conditions, whereas ePMMAs show smaller differences in k_{obs} values at higher pressures (2–4 MPa). Faster rates at 1 MPa may be explained considering that a lower gas pressure applies a milder compression to the polymer chains, thus reducing the shrinking of inter-chain voids or free volume as compared to higher pressures; this leads to a higher diffusivity of CO_2 into the polymer's free volume, as reported in the literature [37]. On the other hand, higher pressures eventually result in higher sorption amounts (Figures 2–4).

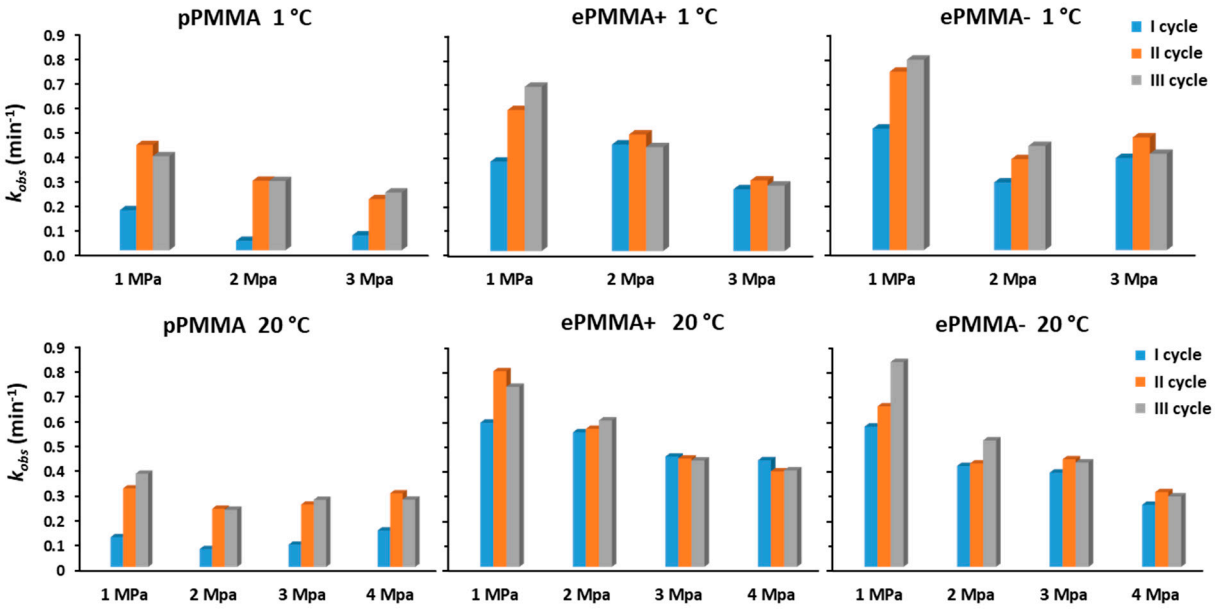

Figure 5. First-order rate constants for CO_2 sorption by PMMAs under the reported conditions.

The durability of ePMMA- was also preliminarily investigated by performing a higher number (i.e., >3) of sorption/desorption cycles using the same polymer specimen. ePMMA- was chosen due to its slightly better handling properties compared to ePMMA+. Figure S9 shows the efficiency loss during consecutive experiments, each obtained after depressurization and equilibration of the polymer sample at the end of the previous cycle. From Figure S9a, it is clear that the CO_2 capture properties of ePMMA- remain unchanged upon repeated use, as the efficiency after the last cycle was only about 5% lower than the first. The efficiency for the nth cycle is defined as (mg of sorbed CO_2 in the nth cycle)/(mg of sorbed CO_2 in the first cycle) × 100.

The possibility of recycling used PMMA was investigated. Spent electrospun PMMAs were obtained by exposing the samples to several cycles of CO_2 sorption–desorption, followed by a regeneration process by melting their fibers and performing electrospinning again on the molten mass. CO_2 sorption experiments carried out on these regenerated fibers show that the carbon dioxide capture performances were superimposable to those observed with ePMMA- obtained from pristine raw materials (Figure S9b).

3.2. Structural Characterization of Electrospun PMMAs

a. AFM

Pristine (i.e., non-previously exposed to CO_2) ePMMA+ fibers showed considerable roughness, with Ra and Rq values of 39.1 nm and 45.9 nm, respectively, which may provide a large gas absorption surface (Figure 6a). Also, the small thickness of the electrospun fibers should allow a very quick sorbing/desorbing of CO_2. The morphology of pristine ePMMA- samples showed a similar profile compared to ePMMA+ with a slight decrease in surface roughness, with values of Ra = 26.4 nm and Rq = 31.7 nm (Figure 6b).

After the first pressure treatment cycle, the ePMMA+ sample showed a more regular and partially "melted" surface, probably due to the plasticizing action of the gas, with the disappearance of the characteristic roughness of the untreated polymer (Figure 6c). A stronger morphological change was observed for exhausted ePMMA-, for which the roughness drastically decreased (Ra = 14.3 nm and Rq = 17.8 nm), making the surface of the fibers very smooth (Figure 6d).

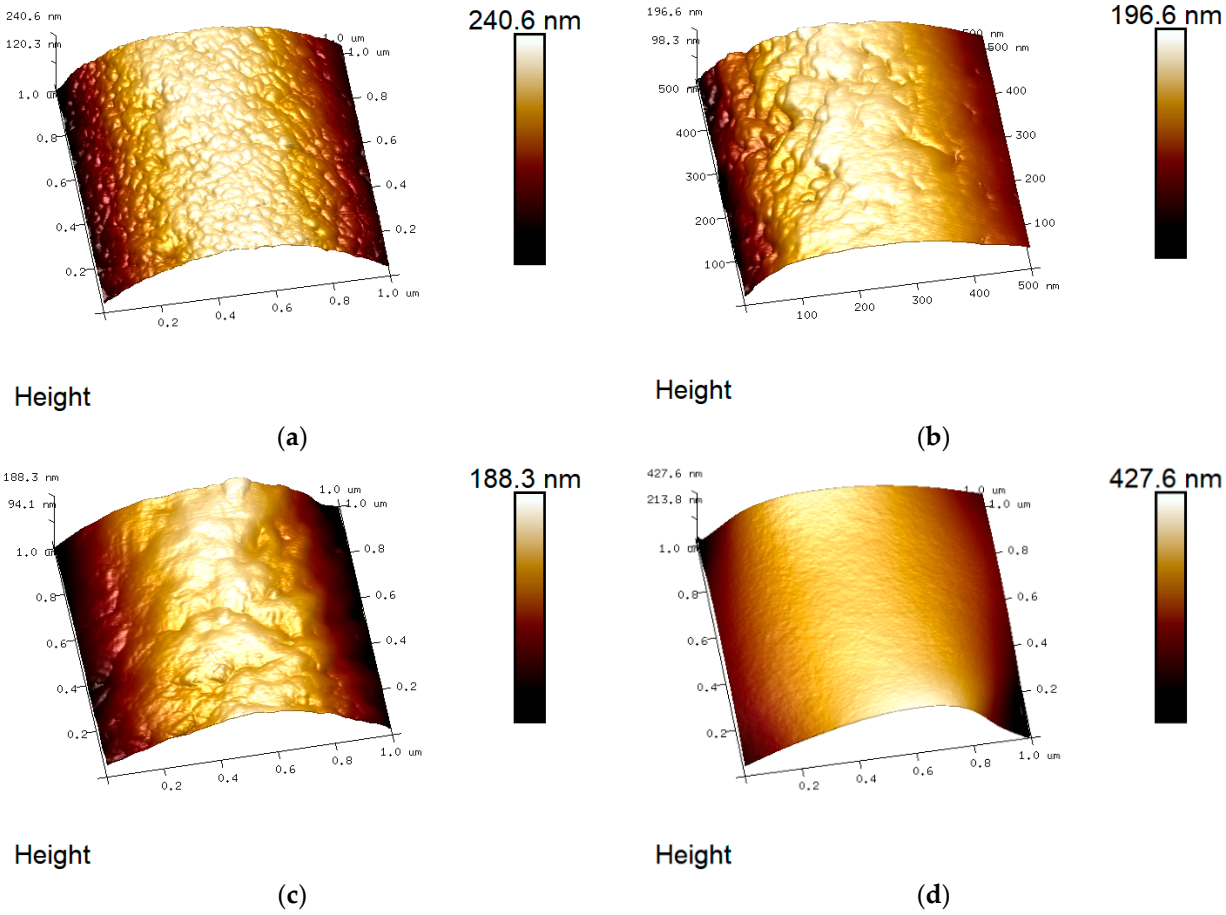

Figure 6. (**a**–**d**): AFM images of pristine ((**a**), top left; (**b**), top right) and spent ((**c**), bottom left; (**d**), bottom right) ePMMA+ and ePMMA- fibers.

b. SEM

Figure 7 shows SEM images of ePMMA+ and ePMMA- under two different magnifications. No major differences were observed between the two species in terms of the morphology of fibers, and average diameters were 1.76 µm and 2.68 µm for ePMMA+ and ePMMA-, respectively. Both materials show a random distribution of the fibers which are homogeneous and free of surface swelling or beads.

c. TGA

Thermogravimetric analysis of electrospun polymers (Figure 8) shows similar degradation kinetics for pPMMA and ePMMA-. It is worth noting that the ePMMA+ tends to lose weight at a slightly faster rate compared to ePMMA- and pPMMA, possibly due to a higher display of hydroxy groups on the outer surface of the fibers. This may be the consequence of a higher surface/volume ratio for ePMMA+ fibers, as determined by an average diameter of ePMMA+ fibers, which is about 35% lower compared to ePMMA- (Figure 7). The observed differences may be explained by recalling that electrospinning modifies the physical state of the bulk polymer by orienting fiber bundles according to the applied tension without affecting the inter-chain chemical bonds (i.e., the dynamic cross-links). Using differential thermal analysis (Figure 8, dashed lines), it is found that two distinctive steps are present for both species. The first step may be related to a structural reorganization with a loss of vinyl unsaturation around 318–329 °C, and the second step is ascribed to the usual decomposition/fragmentation of polymer chains around 429–434 °C. A complete degradation of the polymers is observed before reaching 500 °C.

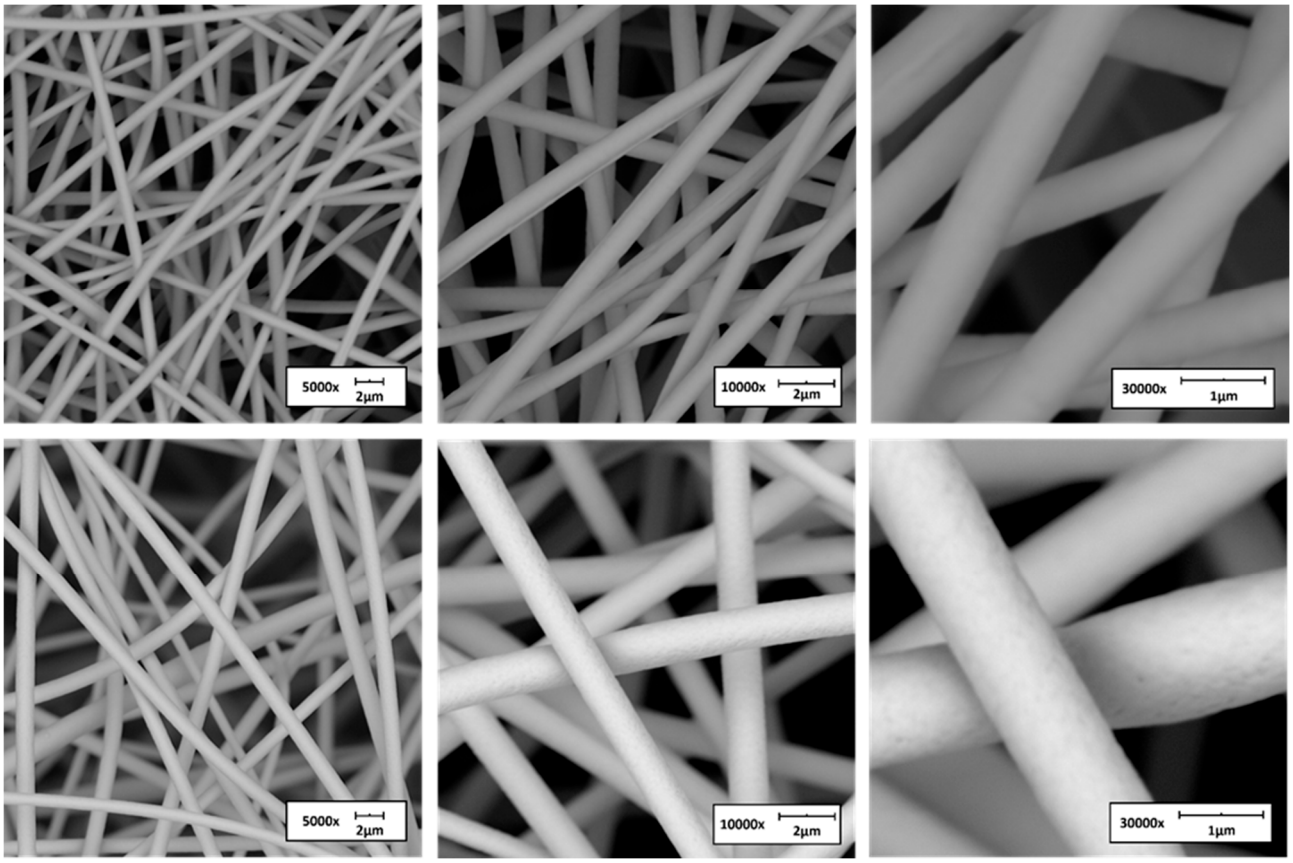

Figure 7. SEM images of ePMMA+ (top row) and ePMMA- (bottom row) at magnifications of 5000×, 10,000× and 30,000×, respectively).

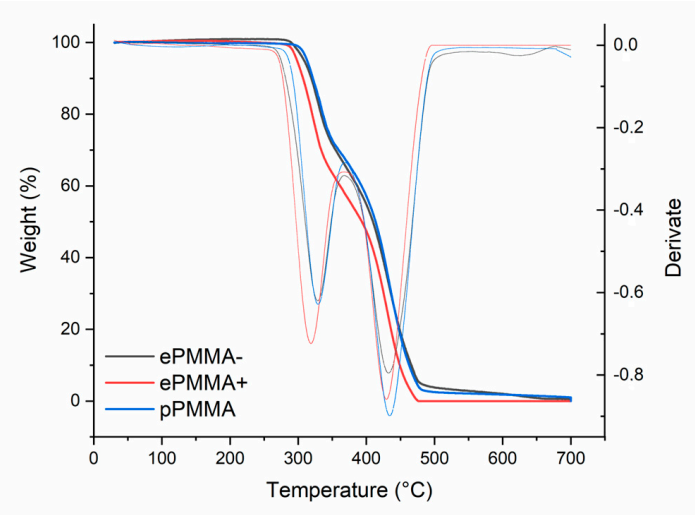

Figure 8. Thermogravimetric analysis of powder and electrospun PMMAs. Dashed lines: DTA profiles for the same species.

d. BET

BET analyses of electrospun PMMAs show a marked difference in the nitrogen sorption/desorption behaviors for the two oppositely charged polymers. ePMMA+ has a monotonic, linear kinetics of nitrogen sorption, which perfectly superimposes with the desorption (Figure 9a), thereby suggesting that pores are easily accessible, and the adsorption and desorption mechanisms occur through the same type of process. On the other hand,

ePMMA- shows a Type 4-like isotherm with an apparent hysteresis between the two curves (Figure 9a) [52]. This difference underlines the importance of the electrospinning process, whereby the same starting material (PMMA) can be worked into end products provided with quite different morphological and functional properties. The observed hysteresis loop for ePMMA- indicates a mesoporous adsorbent where adsorption occurred with capillary condensation [52]. In general, for both samples, the shape of adsorption isotherms indicates a small content of micropores and a significant content of mesopores (pore size 2–50 nm). The apparent surface areas of ePMMA- and ePMMA+ calculated using the BET method in the relative pressure (P/P_0) range from 0.05 to 0.25 are 613.49 m^2 g^{-1} and 519.63 m^2 g^{-1}, respectively (Figure 9b).

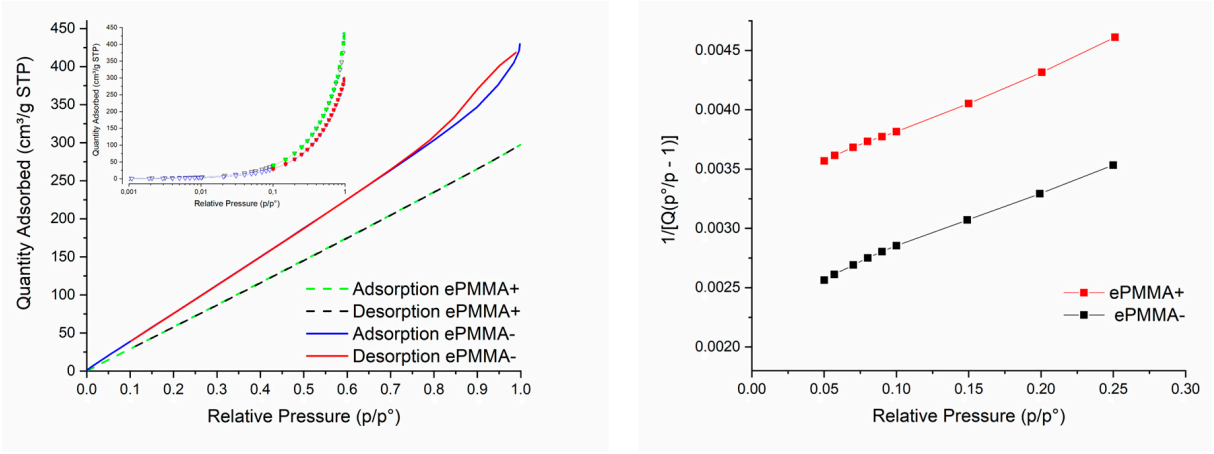

(**a**) (**b**)

Figure 9. ((**a**), left): Isotherms of nitrogen adsorption at 77 K (logarithmic plot in the inset); ((**b**), right): BET surface area plot (the solid line is shown as a guide to the eye).

e. FT-IR

Infrared spectra show that the process of sorption/desorption of carbon dioxide does not modify the chemistry of the backbone and pendant groups of the polymers (Figures S1–S6). They also show that the chemical composition of electrospun PMMAs does not change as compared to pristine PMMA (Figures S7 and S8). The spectra present some typical PMMA features, such as the C−H stretching modes of α-methyl, ester-methyl, and methylene groups at 2900−3000 cm^{-1} and the C-H bendings at 1350–1450 cm^{-1}, as well as the C=O stretching at 1726 cm^{-1} and the three main bands in the 1350–1100 cm^{-1} region of ester group stretching vibrations. The distinctive CO_2 peaks around 2340 cm^{-1} are not present in the post-adsorption spectra, possibly due to at least two processes: (i) pressure release to the ambient atmosphere upon opening of the reactor, and (ii) placing the polymer onto the ATR that lead to a quick release of the gas from the polymer itself.

4. Discussion

The bonding of CO_2 with PMMA is reported as a Lewis acid-base interaction between the oxygen lone pairs in the polymer's carbonyl groups, and the bond dipoles of carbon dioxide [21,25]. This interaction leads to a perturbation of the dynamic cross-links among the polymer chains, thereby promoting their plasticization or rubber transition [26]. Electrospinning treatment of PMMA, while reasonably not affecting this perturbation mechanism, remarkably changes its CO_2-sorption properties in several respects. The first difference is in the kinetic profiles, where pPMMA shows slower sorption kinetics in the first cycle (with a higher plateau value for bound CO_2) compared to subsequent ones. This behavior appears to be generally independent of the pressures and temperatures employed in the experiments. Conversely, electrospun PMMAs provide kinetic parameters of the first sorption profiles, which are broadly superimposable to those of the following cycles, except

at the lower pressure tested (1 MPa). This difference in the sorption behavior of pPMMA and ePMMAs may be partly related to the much higher surface/volume ratio of the latter, whereby plasticization of the polymer surface, which is a known irreversible effect of the action of CO_2 on several synthetic polymers, occurs almost exhaustively during the first sorption cycle across the whole fiber sections, as can be seen from the AFM data and images (Figure 6), which show a reduction in surface roughness caused by plasticization. On the other hand, plasticization may occur less extensively into the core of pPMMA particles due to their larger sizes. Rapid surface plasticization of ePMMAs fibers then results in the observed consistency of the kinetics of CO_2 sorption, as found from the comparison of kinetic rate constants (Figure 5) for sorption cycles I to III under each set of P/T conditions (except at 1 MPa). The observed difference in nitrogen adsorption/desorption mechanisms between ePMMA+ and ePMMA- (see Section 2.d above) is apparently also unimportant when the gas is carbon dioxide instead of nitrogen due to their very different solubility and mechanisms of interaction with the polymer's functional groups. It should also be noted that the present work focuses on a possible application of ePMMAs as CCS media; therefore, sorption/desorption cycles were carried out within short time frames of 60 min for sorption and 30 min for desorption under line vacuum (1.7 kPa). Sorbed CO_2 amounts for ePMMAs reach 90% of plateau values in a matter of seconds (Table S1) and up to three times faster than with pPMMA, thus making these materials reasonably fast for use in membranes for CO_2 separation. It should be noted, however, that exhaustive dissolution of CO_2 into (and desorption from) PMMA may require much longer times, as pointed out by some authors [7,53].

Another difference between pPMMA and ePMMAs relates to the amounts of sorbed CO_2. Under the higher tested pressures of 4 MPa (20 °C) and 3 MPa (1 °C), the weights of CO_2 bound by the ePMMAs are higher by approximately 25% and 30%, respectively, compared to pPMMA under the same conditions. The most interesting finding in this respect is in the amounts of captured CO_2 under the lower pressures, where CO_2 amount of up to 11 times higher was found for ePMMAs compared to pPMMA at 1 MPa (Table 1). This remarkable improvement in capture efficiency under low CO_2 pressures may be particularly beneficial for technological applications, such as in the development of cheap, solid-state devices for CCS. Preliminary results also show a <5% decrease in the amount of sorbed CO_2 after 10 sorption/desorption cycles (Figure S9).

The rationale for higher sorbed CO_2 amounts but slower kinetics as the pressure increases may be found in the opposite effects of hydrostatic pressure and plasticization by a "solvent" gas such as CO_2. An increase in gas pressure causes a mechanical (hydrostatic) effect leading to a reduction of the free volume among polymer chains, which slows down the diffusion of gas molecules into the polymer and promotes vitrification [35,54]. At the same time, CO_2 molecules penetrating the free volumes cause perturbation of dynamic cross-links between adjacent chains, thus accelerating chain mobility and depressing the polymer viscosity and T_g [55–59]. Conversely, at 1 MPa the hydrostatic shrinking of inter-chain spaces is low, thereby promoting the entropically driven filling of voids by CO_2 molecules. This process is very effective when the polymer is spun into micro-fibers such as the ePMMAs while being much less important in pPMMA where the gas mass transfer is inherently hindered by the large cross-section of bulk polymer particles.

As mentioned in the Introduction, PMMA shows a peculiar dependence of its T_g from temperature and CO_2 pressure, which is known as retrograde vitrification. The experiments in the present work were conducted under the glassy region for PMMA, but it should be mentioned that tests carried out at 1 °C/3 MPa are close to the glass-rubber transition curve [12,26,29,30,33,35,36,60,61] Therefore, it should be assumed that sorption kinetics consistently follow a non-Fickian behavior over the range of P/T conditions adopted, but this assumption seems inconsistent with the finding that the first-cycle sorption curves for each P/T couple are markedly different from the following cycles, at least for pPMMA [28]. This phenomenon appears much weaker in ePMMAs, possibly due to their much larger surface-to-volume ratio, and the axial stretching and orientation of the polymer macro-

molecules due to the electrospinning process. Recent studies on the effective glass transition temperature ($T_{g,eff}$) of different grades of PMMA have highlighted the need of determining the $T_{g,eff}$ for each polymer grade, and the development of the present study will follow this suggestion [32]

5. Conclusions

Electrospun PMMAs form micron-sized, electrostatically oriented fibers with a similar arrangement of pendant groups in the inter-chain spaces. The fibers showed a better CO_2 capture performance under high pressures than the pristine PMMA powder, both in terms of sorption kinetics and the amount of sorbed carbon dioxide. Kinetics are 2–3 times faster for ePMMAs than for pPMMA, and this effect has been ascribed to a higher surface-to-volume ratio for the polymeric fibers. The amount of sorbed CO_2 was a function of gas pressure in all PMMA samples, but up to an 11-fold increase in sorbed gas was observed in ePMMAs at the lower tested pressure of 1 MPa, possibly due to the reduction in hydrostatic shrinking of inter-chain voids. The release of CO_2 from the polymer mass under ambient pressure and temperature is extremely quick, which makes these samples very promising for fast carbon dioxide capture/release from high-pressure exhaust gas mixtures, as found in pre-combustion and oxyfuel combustion processes, or from natural gas. A future perspective is the possible implementation of PMMA electrospun fibers into solid-state carbon capture devices.

Supplementary Materials: The following supporting information can be downloaded at: https://www.mdpi.com/article/10.3390/separations10090505/s1, (A) FT-IR characterization of pristine and electrospun PMMAs under CO_2 pre- and post-adsorption conditions. (B) Characterization of the efficiency losses for pristine and regenerated ePMMAs. (C) Comparison of CO_2 saturation times for pPMMA and ePMMAs.

Author Contributions: Conceptualization, V.C. and M.C.; methodology, R.D.W. and P.B.; software, R.D.W.; validation, M.C., V.C. and P.B.; formal analysis, S.P.; investigation, V.C.; resources, M.C.; data curation, P.B. and S.P.; writing—original draft preparation, P.D.P.; writing—review and editing, S.F. and G.S.; visualization, G.S.; supervision, A.F. and S.F.; project administration, P.D.P.; funding acquisition, A.F. All authors have read and agreed to the published version of the manuscript.

Funding: This work was supported by MUR National Innovation Ecosystem-Recovery and Resilience Plan (PNRR) Italy-Vitality (CUP D73C22000840006). P.B. received postdoctoral funding from MUR under the PON "Research and Innovation" 2014–2020 initiative, "Actions IV.6 Green-Research Contracts on 'Green' Topics-D.M. 1062 10/08/2021" (CUP D55F21003080005).

Data Availability Statement: Data is contained within the article or supplementary material.

Acknowledgments: The authors would like to thank Francesco Nobili, Leonardo Sbrascini, Francesco Stoppa, and Gianluigi Rosatelli for making part of their equipment available (TGA, BET, and SEM), and Nadia Barbacane for her help in designing the TOC.

Conflicts of Interest: The authors declare no conflict of interest.

References

1. Nemitallah, M.A.; Habib, M.A.; Badr, H.M.; Said, S.A.; Jamal, A.; Ben-Mansour, R.; Mokheimer, E.M.A.; Mezghani, K. Oxy-fuel combustion technology: Current status, applications, and trends. *Int. J. Energy Res.* **2017**, *41*, 1670–1708. [CrossRef]
2. Madejski, P.; Chmiel, K.; Subramanian, N.; Kuś, T. Methods and Techniques for CO_2 Capture: Review of Potential Solutions and Applications in Modern Energy Technologies. *Energies* **2022**, *15*, 887. [CrossRef]
3. Aghel, B.; Janati, S.; Wongwises, S.; Shadloo, M.S. Review on CO_2 capture by blended amine solutions. *Int. J. Greenh. Gas Control* **2022**, *119*, 103715. [CrossRef]
4. Yu, C.; Jia, Y.; Fang, K.; Qin, Y.; Deng, N.; Liang, Y. Preparation hierarchical porous MOF membranes with island-like structure for efficient gas separation. *J. Memb. Sci.* **2022**, *663*, 121036. [CrossRef]
5. Kadirkhan, F.; Goh, P.S.; Ismail, A.F.; Wan Mustapa, W.N.F.; Halim, M.H.M.; Soh, W.K.; Yeo, S.Y. Recent Advances of Polymeric Membranes in Tackling Plasticization and Aging for Practical Industrial CO_2/CH_4 Applications—A Review. *Membranes* **2022**, *12*, 71. [CrossRef]

6. Wissinger, R.G.; Paulaitis, M.E. Swelling and sorption in polymer–CO_2 mixtures at elevated pressures. *J. Polym. Sci. Part B Polym. Phys.* **1987**, *25*, 2497–2510. [CrossRef]
7. Kim, J.; Kim, K.H.; Ryu, Y.; Cha, S.W. Modeling and Experiment for the Diffusion Coefficient of Subcritical Carbon Dioxide in Poly(methyl methacrylate) to Predict Gas Sorption and Desorption. *Polymers* **2022**, *14*, 596. [CrossRef]
8. Wissinger, R.G.; Paulaitis, M.E. Molecular Thermodynamic Model for Sorption and Swelling in Glassy Polymer-CO_2 Systems at Elevated Pressures. *Ind. Eng. Chem. Res.* **1991**, *30*, 842–851. [CrossRef]
9. Aubert, J.H. Solubility of carbon dioxide in polymers by the quartz crystal microbalance technique. *J. Supercrit. Fluids* **1998**, *11*, 163–172. [CrossRef]
10. Liu, D.; Li, H.; Noon, M.S.; Tomasko, D.L. CO_2-induced PMMA swelling and multiple thermodynamic property analysis using Sanchez-Lacombe EOS. *Macromolecules* **2005**, *38*, 4416–4424. [CrossRef]
11. Webb, K.F.; Teja, A.S. Solubility and diffusion of carbon dioxide in polymers. *Fluid Phase Equilib.* **1999**, *158–160*, 1029–1034. [CrossRef]
12. Kiran, E.; Sarver, J.A.; Hassler, J.C. Solubility and diffusivity of CO_2 and N_2 in polymers and polymer swelling, glass transition, melting, and crystallization at high pressure: A critical review and perspectives on experimental methods, data, and modeling. *J. Supercrit. Fluids* **2022**, *185*, 105378. [CrossRef]
13. Vopička, O.; De Angelis, M.G.; Du, N.; Li, N.; Guiver, M.D.; Sarti, G.C. Mixed gas sorption in glassy polymeric membranes: II. CO_2/CH_4 mixtures in a polymer of intrinsic microporosity (PIM-1). *J. Memb. Sci.* **2014**, *459*, 264–276. [CrossRef]
14. Notario, B.; Pinto, J.; Rodríguez-Pérez, M.A. Towards a new generation of polymeric foams: PMMA nanocellular foams with enhanced physical properties. *Polymers* **2015**, *63*, 116–126. [CrossRef]
15. Shi, Z.; Ma, X.; Zhao, G.; Wang, G.; Zhang, L.; Li, B. Fabrication of high porosity Nanocellular polymer foams based on PMMA/PVDF blends. *Mater. Des.* **2020**, *195*, 109002. [CrossRef]
16. Kwon, Y.K.; Bae, H.K. Production of microcellular foam plastics by supercritical carbon dioxide. *Korean J. Chem. Eng.* **2007**, *24*, 127–132. [CrossRef]
17. Koros, W.J.; Smith, G.N.; Stannett, V. High-pressure sorption of carbon dioxide in solvent-cast poly(methyl methacrylate) and poly(ethyl methacrylate) films. *J. Appl. Polym. Sci.* **1981**, *26*, 159–170. [CrossRef]
18. Fried, J.R.; Li, W. High-pressure FTIR studies of gas–polymer interactions. *J. Appl. Polym. Sci.* **1990**, *41*, 1123–1131. [CrossRef]
19. Edwards, R.R.; Tao, Y.; Xu, S.; Wells, P.S.; Yun, K.S.; Parcher, J.F. Chromatographic investigation of CO_2-polymer interactions at near-critical conditions. *J. Phys. Chem. B* **1998**, *102*, 1287–1295. [CrossRef]
20. Shoghl, S.N.; Pazuki, G.; Raisi, A. A model to predict the solubility and permeability of gaseous penetrant in the glassy polymeric membrane at high pressure. *J. Appl. Polym. Sci.* **2021**, *138*, 50548. [CrossRef]
21. Nelson, M.R.; Borkman, R.F. Ab initio calculations on CO_2 binding to carbonyl groups. *J. Phys. Chem. A* **1998**, *102*, 7860–7863. [CrossRef]
22. Shieh, Y.T.; Liu, K.H. The effect of carbonyl group on sorption of CO_2 in glassy polymers. *J. Supercrit. Fluids* **2003**, *25*, 261–268. [CrossRef]
23. Takahashi, M.; Yamamoto, Y.; Nawaby, A.V.; Handa, Y.P. Raman spectroscopic investigation of the phase behavior and phase transitions in a poly(methyl methacrylate)-carbon dioxide system. *J. Polym. Sci. Part B Polym. Phys.* **2003**, *41*, 2214–2217. [CrossRef]
24. Shieh, Y.T.; Liu, K.H. Solubility of CO_2 in glassy PMMA and PS over a wide pressure range: The effect of carbonyl groups. *J. Polym. Res.* **2002**, *9*, 107–113. [CrossRef]
25. Ricci, E.; De Angelis, M.G.; Minelli, M. A comprehensive theoretical framework for the sub and supercritical sorption and transport of CO_2 in polymers. *Chem. Eng. J.* **2022**, *435*, 135013. [CrossRef]
26. Di Noto, V.; Vezzù, K.; Giffin, G.A.; Conti, F.; Bertucco, A. Effect of high pressure CO_2 on the structure of PMMA: A FT-IR study. *J. Phys. Chem. B* **2011**, *115*, 13519–13525. [CrossRef] [PubMed]
27. Kamiya, Y.; Mizoguchi, K.; Terada, K.; Fujiwara, Y.; Wang, J.S. CO_2 sorption and dilation of poly(methyl methacrylate). *Macromolecules* **1998**, *31*, 472–478. [CrossRef]
28. Yoon, J.H.; Kawamura, T.; Takeya, S.; Jin, S.; Yamamoto, Y.; Komai, T.; Takahashi, M.; Nawaby, A.V.; Handa, Y.P. Probing fickian and non-fickian diffusion of CO_2 in poly(methyl methacrylate) using in situ Raman spectroscopy and microfocus X-ray computed tomography. *Macromolecules* **2004**, *37*, 9302–9304. [CrossRef]
29. Wissinger, R.G.; Paulaitis, M.E. Glass transitions in polymer / CO_2 mixtures at elevated pressures. *J. Polym. Sci. Part B Polym. Phys.* **1991**, *29*, 631–633. [CrossRef]
30. Condo, P.D.; Johnston, K.P. In situ measurement of the glass transition temperature of polymers with compressed fluid diluents. *J. Polym. Sci. Part B Polym. Phys.* **1994**, *32*, 523–533. [CrossRef]
31. Baldanza, A.; Loianno, V.; Mensitieri, G.; Scherillo, G. Modelling changes in glass transition temperature in polymer matrices exposed to low molecular weight penetrants. *Philos. Trans. R. Soc. A Math. Phys. Eng. Sci.* **2023**, *381*, 20210216. [CrossRef] [PubMed]
32. Rodríguez, D.C.; Carrascal, D.; Solórzano, E.; Pérez, M.A.R.; Pinto, J. Analysis of the retrograde behavior in PMMA-CO_2 systems by measuring the (effective) glass transition temperature using refractive index variations. *J. Supercrit. Fluids* **2021**, *170*, 105159. [CrossRef]

33. Handa, Y.P.; Zhang, Z. A new technique for measuring retrograde vitrification in polymer-gas systems and for making ultramicrocellular foams from the retrograde phase. *J. Polym. Sci. Part B Polym. Phys.* **2000**, *38*, 716–725. [CrossRef]
34. Guo, H.; Kumar, V. Solid-state poly(methyl methacrylate) (PMMA) nanofoams. Part I: Low-temperature CO_2 sorption, diffusion, and the depression in PMMA glass transition. *Polymers* **2015**, *57*, 157–163. [CrossRef]
35. Condo, P.D.; Sanchez, I.C.; Panayiotou, C.G.; Johnston, K.P. Glass Transition Behavior Including Retrograde Vitrification of Polymers with Compressed Fluid Diluents. *Macromolecules* **1992**, *25*, 6119–6127. [CrossRef]
36. Condo, P.D.; Johnston, K.P. Retrograde Vitrification of Polymers With Compressed Fluid Diluents: Experimental Confirmation. *Macromolecules* **1992**, *25*, 6730–6732. [CrossRef]
37. Mohammadi, M.; Fazli, H.; Karevan, M.; Davoodi, J. The glass transition temperature of PMMA: A molecular dynamics study and comparison of various determination methods. *Eur. Polym. J.* **2017**, *91*, 121–133. [CrossRef]
38. Li, R.; Zhang, Z.; Fang, T. Experimental research on swelling and glass transition behavior of poly(methyl methacrylate) in supercritical carbon dioxide. *J. Supercrit. Fluids* **2016**, *110*, 110–116. [CrossRef]
39. Ikeda-Fukazawa, T.; Kita, D.; Nagashima, K. Raman spectroscopic study of CO_2 sorption process in poly methyl methacrylate. *J. Polym. Sci. Part B Polym. Phys.* **2008**, *46*, 831–842. [CrossRef]
40. Braeuer, A.S. Prospects: Facing current challenges in high pressure high temperature process engineering with in situ Raman measurements. *J. Supercrit. Fluids* **2018**, *134*, 80–87. [CrossRef]
41. Tsioptsias, C.; Panayiotou, C. Simultaneous determination of sorption, heat of sorption, diffusion coefficient and glass transition depression in polymer-CO_2 systems. *Thermochim. Acta.* **2011**, *521*, 98–106. [CrossRef]
42. Eslami, H.; Kesik, M.; Karimi-Varzaneh, H.A.; Müller-Plathe, F. Sorption and diffusion of carbon dioxide and nitrogen in poly(methyl methacrylate). *J. Chem. Phys.* **2013**, *139*, 124902. [CrossRef]
43. Taguchi, T.; Saito, H. Effects of plasticization and hydrostatic pressure on tensile properties of PMMA under compressed carbon dioxide and nitrogen. *J. Appl. Polym. Sci.* **2016**, *133*, 43431. [CrossRef]
44. Tang, Q.; Yang, B.; Zhao, Y.; Zhao, L. Sorption and diffusion of sub/supercritical carbon dioxide in poly(methyl methacrylate). *J. Macromol. Sci. Part B Phys.* **2007**, *46*, 275–284. [CrossRef]
45. Zhou, L.; Dai, X.; Du, J.; Wang, T.; Wu, L.; Tang, Y.; Shen, J. Fabrication of Poly(MMA- co -ST) Hybrid Membranes Containing AgCl Nanoparticles by in Situ Ionic Liquid Microemulsion Polymerization and Enhancement of Their Separation Performance. *Ind. Eng. Chem. Res.* **2015**, *54*, 3326–3332. [CrossRef]
46. Shen, J.-N.; Zheng, X.-C.; Ruan, H.-M.; Wu, L.-G.; Qiu, J.-H.; Gao, C.-J. Synthesis of AgCl/PMMA hybrid membranes and their sorption performance of cyclohexane/cyclohexene. *J. Memb. Sci.* **2007**, *304*, 118–124. [CrossRef]
47. Maroni, F.; Bruni, P.; Suzuki, N.; Aihara, Y.; Croce, F. Electrospun tin-carbon nanocomposite as anode material for all solid state lithium-ion batteries. *J. Solid State Electrochem.* **2019**, *23*, 1697–1703. [CrossRef]
48. Di Profio, P.; Canale, V.; D'Alessandro, N.; Germani, R.; Di Crescenzo, A.; Fontana, A. Separation of CO_2 and CH_4 from Biogas by Formation of Clathrate Hydrates: Importance of the Driving Force and Kinetic Promoters. *ACS Sustain. Chem. Eng.* **2017**, *5*, 1990–1997. [CrossRef]
49. Canale, V.; Fontana, A.; Siani, G.; Di Profio, P. Hydrate Induction Time with Temperature Steps: A Novel Method for the Determination of Kinetic Parameters. *Energy Fuels* **2019**, *33*, 6113–6118. [CrossRef]
50. Arca, S.; Di Profio, P.; Germani, R.; Savelli, G. Apparatus for Preparing and Studying Clathrate Hydrates. WO2007122647A1, 21 April 2006.
51. Gazzani, M.; Macchi, E.; Manzolini, G. CO_2 capture in natural gas combined cycle with SEWGS. Part A: Thermodynamic performances. *Int. J. Greenh. Gas Control* **2013**, *12*, 493–501. [CrossRef]
52. Thommes, M.; Kaneko, K.; Neimark, A.V.; Olivier, J.P.; Rodriguez-Reinoso, F.; Rouquerol, J.; Sing, K.S.W. Physisorption of gases, with special reference to the evaluation of surface area and pore size distribution (IUPAC Technical Report). *Pure Appl. Chem.* **2015**, *87*, 1051–1069. [CrossRef]
53. Chiou, J.S.; Paul, D.R. Effects of CO_2 exposure on gas transport properties of glassy polymers. *J. Memb. Sci.* **1987**, *32*, 195–205. [CrossRef]
54. Miranda, L.D.; Bell, R.J.; Short, R.T.; van Amerom, F.H.W.; Byrne, R.H. The influence of hydrostatic pressure on gas diffusion in polymer and nano-composite membranes: Application to membrane inlet mass spectrometry. *J. Memb. Sci.* **2011**, *385–386*, 49–56. [CrossRef]
55. Neyertz, S.; Brown, D. Molecular dynamics study of carbon dioxide sorption and plasticization at the interface of a glassy polymer membrane. *Macromolecules* **2013**, *46*, 2433–2449. [CrossRef]
56. Hirota, S.I.; Tominaga, Y.; Asai, S.; Sumita, M. Dielectric relaxation behavior of poly(methyl methacrylate) under high-pressure carbon dioxide. *J. Polym. Sci. Part B Polym. Phys.* **2005**, *43*, 2951–2962. [CrossRef]
57. Zhang, Z.; Handa, Y.P. An in situ study of plasticization of polymers by high-pressure gases. *J. Polym. Sci. Part B Polym. Phys.* **1998**, *36*, 977–982. [CrossRef]
58. Kwag, C.; Manke, C.W.; Gulari, E. Rheology of molten polystyrene with dissolved supercritical and near-critical gases. *J. Polym. Sci. Part B Polym. Phys.* **1999**, *37*, 2771–2781. [CrossRef]
59. Gutiérrez, C.; Rodríguez, J.F.; Gracia, I.; de Lucas, A.; García, M.T. Modification of polystyrene properties by CO_2: Experimental study and correlation. *J. Appl. Polym. Sci.* **2015**, *132*, 41696. [CrossRef]

60. Kalospiros, N.S.; Paulaitis, M.E. Molecular thermodynamic model for solvent-induced glass transitions in polymer—Supercritical fluid systems. *Chem. Eng. Sci.* **1994**, *49*, 659–668. [CrossRef]
61. Chiou, J.S.; Barlow, J.W.; Paul, D.R. Plasticization of glassy polymers by CO_2. *J. Appl. Polym. Sci.* **1985**, *30*, 2633–2642. [CrossRef]